Chapter 7
A Statistical Theory of Dendritic Morphology

Quan Wen

Abstract Since Santiago Ramon y Cajal, neuroscientists have been fascinated by the shapes of dendritic arbors for more than 100 years. However, the principle underlying these complex and diverse structures remains elusive. Here we propose that evolution has tinkered with brain design to maximize its functionality while minimizing the cost associated with building and maintaining it. We hypothesize that the functionality of a neuron benefits from a larger repertoire of connectivity patterns between dendrites and surrounding axons, and the cost of a dendritic arbor increases with its total length and path length from synapses to soma. We solved this optimization problem by drawing an analogy with maximization of the entropy for a given energy in statistical physics. The solution predicts several scaling relationships between arbor dimensions and closely fits with experimental data. Moreover, our theory may explain why basal dendrites of pyramidal cells and Purkinje cells, the two major cell types in the mammalian brains, exhibit distinct morphologies.

7.1 Introduction

Studying the structure of an organ helps unravel its function. More than 100 years ago, by applying the histological staining technique to study the anatomy of nervous systems, Santiago Ramon y Cajal formulated the "neuron doctrine." He proposed that neurons are interconnected with each other by two polarized components, axons and dendrites. The function of dendrites and axons is to conduct electrical signals from postsynaptic terminals to the integration site, which often is the cell body, and from the integration site to the presynaptic terminals, respectively.

Q. Wen (✉)
Department of Physics and Center for Brain Science, Harvard University,
17 Oxford Street, Cambridge, MA 02138, USA
e-mail: vineygeyser@gmail.com

H. Cuntz et al. (eds.), *The Computing Dendrite: From Structure to Function*,
Springer Series in Computational Neuroscience 11, DOI 10.1007/978-1-4614-8094-5_7,

One hundred years later, neurobiologists, armed with advanced tools, are embracing a great opportunity to dissect the complex structure of the neuronal circuitry. For instance, cell-labeling methods such as those based on biocytin or green fluorescent protein make it possible to describe neuronal arbors in a comprehensive and quantitative way (Ascoli 2006). Reconstructing the wiring diagram of an entire brain circuitry may become an attainable goal with the advances of high-throughput electron microscopy and computer-aided image analysis (Lichtman et al. 2008; Denk and Horstmann 2004; Chklovskii et al. 2010; Kleinfeld et al. 2011). However, a quantitative theory of neuronal arbor shape does not exist. By establishing a direct relationship between neuronal structure and function, such a theory could elucidate the design principles of neural circuit.

Insight in this direction was also contributed by Cajal, as he wrote (Ramón y Cajal 1899), "After the many shapes assumed by neurons, we are now in a position to ask whether this diversity … has been left to chance and is insignificant, or whether it is tightly regulated and provides an advantage to the organism. … we realized that all of the various conformations of the neuron and its various components are simply morphological adaptations governed by laws of conservation for time, space, and material."

Echoing Cajal's thoughts, we propose that evolution has "tinkered" with the brain design to maximize the functionality of a neuronal arbor while minimizing the cost associated with building and maintaining it. Specifically, brain functionality must benefit from high synaptic connectivity and large plasticity, because synaptic connections are central to information processing as well as learning and memory. However, increasing connectivity requires adding wiring to the network, which comes at a cost. The cost of wiring could be accrued by various things, including conduction delays, signal attenuation, and wiring volume. Below, I will show that these ideas can be formulated in the framework of constrained optimization. By solving this mathematical problem, we can account for several salient features of the shape of pyramidal and Purkinje dendritic arbors, the two major cell types in mammalian brains. This chapter is based on two papers that I have published earlier (Wen and Chklovskii 2008; Wen et al. 2009).

7.2 Dendritic Cost Function and Potential Connectivity Constraints

To start, let us consider the cost of wiring. We assume that the cost of dendritic arbors E grows with the total dendritic length L, i.e., $\partial E/\partial L > 0$, and with the average path length from a synapse to the soma l, i.e., $\partial E/\partial l > 0$ for all L and l. The path length cost may be contributed by several factors such as longer delays and greater attenuation of synaptic signals and higher metabolic costs for intracellular transport (Cuntz et al. 2007; Wen and Chklovskii 2008). These two quite general assumptions will be sufficient to make predictions about optimal dendritic shape, which I will then compare with the shape of purkinje dendritic arbors in the cerebellum.

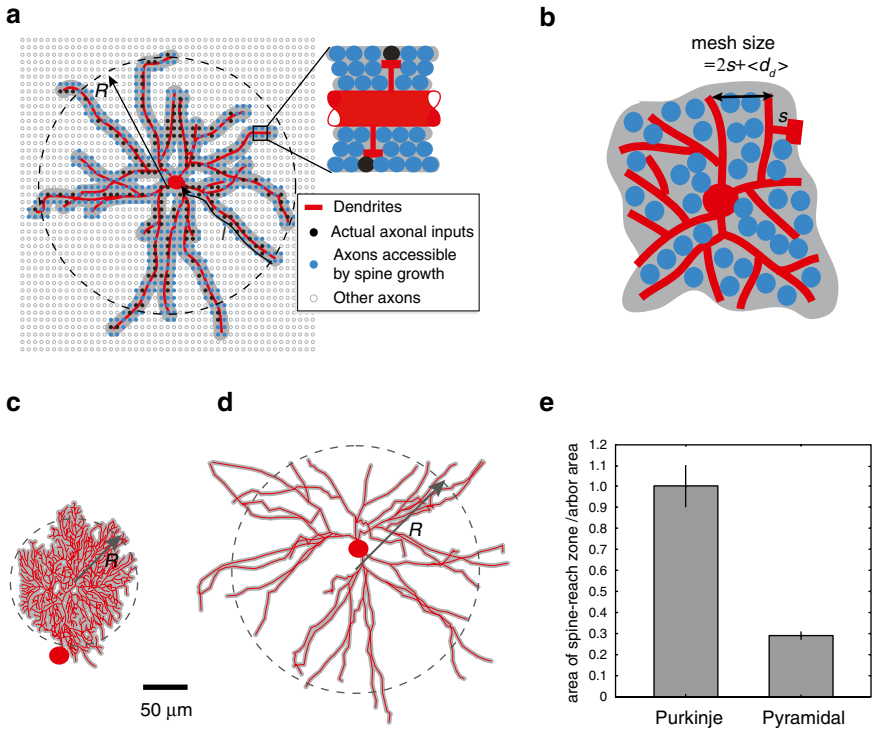

Fig. 7.1 The shape of a dendritic arbor determines which axons are accessible to a neuron. (**a**) Schematic illustration of a 3D dendritic arbor projected onto a plane and nearby axons that are labelled based on their relations to the arbor. For illustration purposes, we have shown all axons as running orthogonally to the plane of the drawing. Actual synapses (*black dots*) are a subset of potential synapses (*solid blue circles*), which in turn are chosen out of a larger set of axons (*circles*). Potential synapses are located within the spine-reach zone of a dendrite (*gray*). (**b**) A compact branching arbor makes on average one potential synapse with each axon (*blue*) passing through the arbor. The mesh size is defined as the arbor area divided by the total dendritic length. The mesh size is $2s+\langle d_d \rangle$ for a compact planar arbor and is the same, up to a numerical factor of order one, for a compact 3D arbor. (**c**) Dendritic arbor of a Purkinje cell from mouse cerebellum and its spine-reach zone. (**d**) Basal dendritic arbor (*red*) of a pyramidal cell from rat cortex (Shepherd and Svoboda 2005) and its spine-reach zone (*gray*). The arbor territory is approximated by the *dashed circle*. (**e**) Ratio of the area of the spine-reach zone to the area of the arbor territory on a 2D projection [$n=10$ for both pyramidal and Purkinje cells (Kisvarday and Eysel 1992; Martone et al. 2003; Ascoli 2006; Rapp et al. 1994; Vetter et al. 2001)]. The spine-reach zone area is calculated as $2sL$, where $s=2$ µm. Pyramidal basal dendrites are sparser than Purkinje dendrites ($p<10^{-5}$, t-test with unequal variances) and, therefore, have lower probability to form a potential synapse with an axon passing through its territory. Error bars are s.e.m. These digitally reconstructed arbors are publically accessible from http://NeuroMorpho.Org [see also (Ascoli 2006)]. This figure is modified from Wen et al. (2009)

Next, we switch our attention to the constraints. We consider wiring up a neural circuit for a fixed number of potential synapses per neuron. We define *potential synapse* as a location where an axon passes within a spine length of a dendrite (Fig. 7.1a and Stepanyants et al. 2002). A potential synapse can be converted into an actual one by growing a spine (Trachtenberg et al. 2002). Requiring a potential

convergence factor imposes the following constraints on L and l. For simplicity, let us first consider a planar dendritic arbor and axons running orthogonally to it. C axons must fit within a spine length s of a dendrite, which we call the spine-reach zone (gray area in Fig. 7.1a). Then, the area of the spine-reach zone ($2sL$) must be at least equal to the total cross-sectional area of the axons ($\pi/4Cd_a^2$), where d_a is the axon diameter.

Likewise, the mean path length l can only be greater or on the same order of linear arbor radius R. We define R as the root-mean-square distance from the center mass of the arbor to all dendritic segments. A planar arbor must at least encompass all the potential axons and the area occupied by the dendrites on the plane.

7.3 Optimal Dendritic Arbor Is Planar, Compact, and Centripetal

By minimizing the cost function E subject to the constraints of L and l, it is straightforward to show that the total dendritic length and path length satisfy (Wen and Chklovskii 2008)

$$L = \frac{\pi}{4} C d_a^2 / 2s. \tag{7.1}$$

$$l \sim R. \tag{7.2}$$

Here approximately (~) suggests that l and R only differ by a numerical factor that is close to one. In addition, in an optimal arbor, the total arbor area A should satisfy

$$A = \frac{\pi}{4} C d_a^2 \left(1 + d_d / 2s\right). \tag{7.3}$$

In (7.3), $\langle d_d \rangle$ is the mean dendritic diameter. Dendritic arbors satisfying (7.1)–(7.3) have the following properties. First, minimizing total dendritic length ((7.1)) demands a spatial organization of the neuropil, in which adjacent dendrites from different neurons are excluded from each other's spine-reach zone (Fig. 7.1a, inset). If dendrites penetrated each other's spine-reach zones, they would add to the excluded volume of axons and would increase the total dendritic length.

Second, to achieve the minimum path length l in (7.2), each segment of the dendrite should be directed towards the soma. We call such arbor design centripetal (Fig. 7.1a). If the total dendritic length is greater than the dendritic arbor span, the centripetal arbor must branch. Therefore, branching of dendrites is a trivial consequence of minimizing the mean path length.

In suboptimal dendritic arbors, the dependence of l on R does not have to be linear as suggested by (7.2). For example, if dendrites consisted of randomly oriented segments, like in a random walk, the path length would be $l \sim R^2$.

Third, we calculate the arbor mesh size—a parameter that quantifies the sparseness of an arbor—by dividing the arbor area by the total length, A/L. By combining (7.1) and (7.3), we find that

$$\frac{A}{L} = 2s + d_d. \tag{7.4}$$

We call an arbor satisfying (7.4) compact (Fig. 7.1b). One property of a compact arbor is that it forms on average one potential synapse with each axon passing through the arbor.

A compact branching arbor is less costly than other branching arbors with the same potential convergence. Consider a sparse arbor with a mesh size that is much larger than $2s + \langle d_d \rangle$ (Fig. 7.1a) and which does not form potential synapses with every axon passing through the arbor (Fig. 7.1a). A compact arbor is less costly because it has smaller span than a sparse branching arbor.

How does this analysis of a planar dendritic arbor generalize to 3D dendritic arbors and axons running in different directions? Note that we can always project a 3D dendritic arbor onto a plane that is orthogonal to the running direction of some axons. One can then calculate the spine-reach zone area that captures these axons. The same procedure can be performed on different arbor projections, and the sum of these spine-reach zone areas will determine the total dendritic length and the arbor size. Direct calculation shows that in the 3D case, the optimality conditions still hold if numerical factors close to one are ignored. Yet when these numerical factors are included, a planar arbor is preferable because a 2D projection of a 3D arbor is always shorter than the original. Thus, both the minimum path length, l, and the minimum total dendritic length, L, in a planar arbor are shorter than those in a 3D arbor.

7.4 Purkinje Dendritic Arbors Are Planar, Compact, and Centripetal

In the previous section, we derived the properties of optimal dendritic arbors that minimize cost for a given potential connectivity. Next, we compare our predictions with the experimental measurements for Purkinje dendritic arbors. As Purkinje arbors are evidently planar, we demonstrate that they are compact and centripetal.

To prove that Purkinje dendritic arbors are compact, we refer to (7.4) and show that the mesh size of a dendritic arbor is $2s + \langle d_d \rangle$. Napper and Harvey (1988b) reported that $s = 1.4$ μm as measured from the surface of the dendrites to the tip of the spine. They also found the diameter of spiny dendrites receiving parallel fiber inputs to be $\langle d_d \rangle = 1.5$ μm. Dividing the arbor area by the total dendritic length yields a value close to 4 μm (Fig. 7.1c, e), which is consistent with (7.4).

To demonstrate that Purkinje cell dendrites are centripetal, we calculated the distribution of dendritic segment orientation angle θ (Fig. 7.2a), which is defined as the angle between the vector of the signal flowing along a dendritic segment and the vector pointing centripetally from the segment to the soma. Figure 7.2b shows a Purkinje dendritic arbor where each dendritic segment is colored according to the

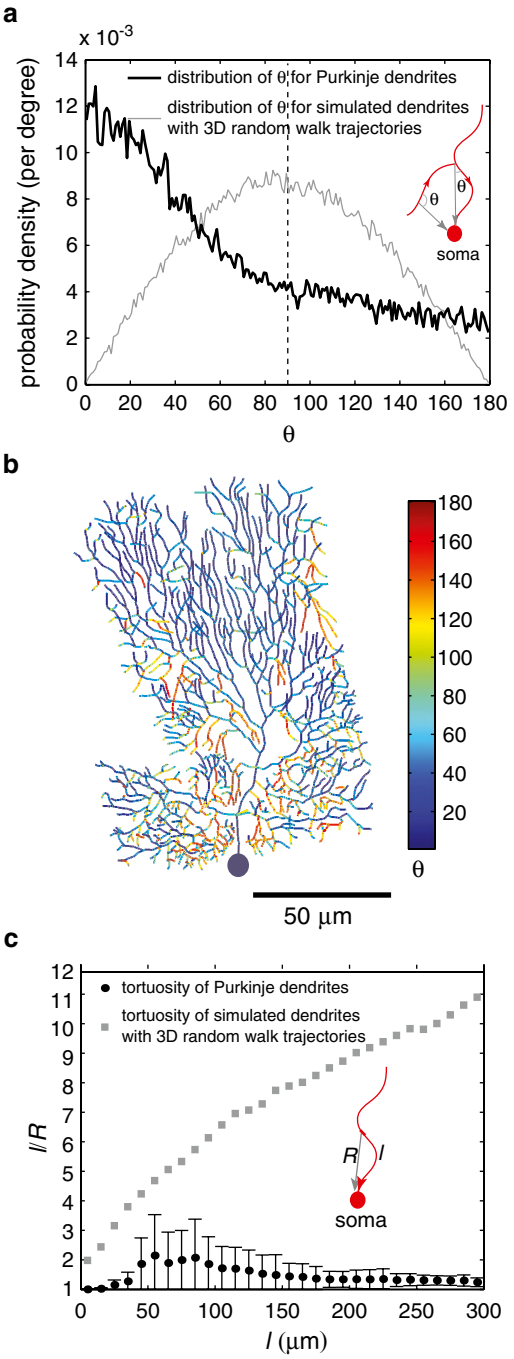

Fig. 7.2 Purkinje dendritic arbors are centripetal. (**a**) The probability distribution of the orientation angle θ between the vector associated with a Purkinje dendritic segment and the vector pointing centripetally from the segment to the soma (*black line*). Seventy percent of the segments have angles less than 90° (the total area under the *black curve* from 0 to 90°). *Gray line* is the probability distribution of angles for dendritic branches generated by 3D random walk trajectories.

value of θ. We found that 70 % of the segments have orientation angles less than 90° (Fig. 7.2a), which suggests that Purkinje dendritic segments are predominately centripetal. This observation is consistent with the measurements of pyramidal cell dendrites in hippocampus (Samsonovich and Ascoli 2003).

Many trajectories observed in nature are not centripetal, and one of the classical examples is a random walk. For comparison, we simulated a random walk comprising rigid segments 5 μm in length with random orientations and plotted the probability distribution of orientation angles (gray line in Fig. 7.2a). In a 2D random walk, the orientation angle would have a uniform distribution. However, in a 3D random walk, the most likely orientation angle is near 90° (Fig. 7.2a).

In optimal dendrites, the typical path length from a dendritic segment to the soma must be close to the Euclidean distance between them (7.2), i.e., the tortuosity index, defined as the ratio of the path length from a dendritic segment to the soma to the Euclidean distance between the two locations, is close to one. To verify that dendrites are optimal, we plot the tortuosity in Purkinje cell dendrites as a function of path length (Fig. 7.2c). Unlike the simulated dendrites with random walk trajectories, the tortuosity of real dendrites is close to one (Fig. 7.2c), consistent with optimality.

7.5 Micro-Architecture of the Cerebellum Molecular Layer

To verify that Purkinje cell dendrites from different neurons are excluded from each other's spine-reach zone (Fig. 7.1a, inset), we shall estimate the interval b between potential synapses along a parallel fiber in the molecular layer and show that $b = 2s + \langle d_d \rangle$ (Napper and Harvey 1988a).

We can view the interval b as the distance a parallel fiber travels before encountering a different Purkinje dendrite. Along its course, a parallel fiber with length L_a will encounter totally D different dendrites and $b = L_a/D$. Below I will call D the potential divergence factor of an axon, and it can be calculated as follows. Because Purkinje cell dendrites are compact, an axon can potentially connect with all the dendrites in the volume $L_a wh$, where w is the width of the dendritic arbor and h is the height of the arbor. Therefore, we have

$$D = \sigma L_a wh, \tag{7.5}$$

Fig. 7.2 (continued) Random walk is not centripetal as the distribution has a peak near 90°. (**b**) A digitized Purkinje dendritic arbor, where the color of each dendritic segment represents the value of the orientation angle. (**c**) The tortuosity of Purkinje cell dendrites, which is defined as the ratio of the path length from the soma to a dendritic segment to the Euclidian distance between the two locations, is close to one for different path lengths from dendritic segments to the soma. The tortuosity of dendrites generated by random walk trajectories is much higher than that of Purkinje cell dendrites, and it scales with the square root of the path length. All error bars are standard deviations. The above analysis is done on ten digitally reconstructed Purkinje dendritic arbors (Rapp et al. 1994; Vetter et al. 2001; Martone et al. 2003) available from http://neuromorpho.org. The arbors were projected onto the plane perpendicular to the parallel fibers (*sagittal plane*). This figure is modified from Wen and Chklovskii (2008)

where ρ is the neuronal density. Because Purkinje cell bodies are arranged uniformly in a layer, we may rewrite (7.5) as a function of the neuronal density per unit area σ,

$$D = \sigma L_a w. \tag{7.6}$$

As a result, the interval of potential synapses on an axon b is given by

$$b = L_a / D = \frac{1}{\sigma w}. \tag{7.7}$$

By substituting the values from the rat cerebellum $\sigma = 1{,}018\ \text{mm}^{-2}$, $w = 250\ \mu\text{m}$, we obtain $b = 4\ \mu\text{m}$. Recalling that $s = 1.4\ \mu\text{m}$ and $d_d = 1.5\ \mu\text{m}$ (Napper and Harvey 1988b), we find that the relation $b = 2s + d_d$ is satisfied and adjacent Purkinje cell dendrites are on average excluded from each other's spine-reach zone. We hope this calculation can be verified directly by electron microscopic reconstructions.

7.6 Purkinje and Pyramidal Dendritic Arbors Exhibit Distinct Morphologies

Although we were able to explain the shape of Purkinje cell dendrites, neuronal arbor shape varies among cell classes. In particular, cortical pyramidal cell dendrites in the neocortex have 3D shape and are sparser than Purkinje cell dendrites on a projection: the distance between adjacent branches is much greater than spine length (Fig. 7.1d). How can we understand the shape of such dendrites?

One difference between the Purkinje cells in the cerebellum and the pyramidal cells in the cortex is the geometry of axons representing their dominant input. Unlike parallel fibers in the cerebellum, cortical axons run in different directions. Thus, a flat dendritic arbor can effectively capture only those axons that are oriented near orthogonally to the dendritic plane while a 3D dendritic arbor can effectively capture axons from all directions. However, the sparseness of pyramidal cells suggests that they are not minimizing their dendritic cost. Instead, understanding the shape of pyramidal dendrites requires the introduction of a new principle.

7.7 Maximizing the Connectivity Repertoire as a Statistical Principle

Mammalian neocortex is a highly plastic brain region vital for learning and memory. Because the shape of a dendritic arbor determines which axons are accessible to which dendrites, we hypothesize that the sparseness of a pyramidal dendritic arbor may reflect its flexibility to find appropriate presynaptic neurons. In an adult brain, a dendritic arbor connects with a combination of appropriate neurons, whose axons are sparsely distributed [constituting less than 10 % of all axons

passing through the arbor territory (Stepanyants et al. 2002; Markram et al. 1997; Thomson and Bannister 2003; Sjöström et al. 2001)] and are not known to the dendrites prior to arbor growth. In the course of neuronal development, the arbor must find this combination in the ensemble of accessible input neuron combinations (via physical contacts between axons and dendrites) defined by arbor dimensions. Then, finding a more appropriate combination would require choosing arbor dimensions that have a larger ensemble. Furthermore, if the developmental search strategy is sufficiently good, the larger the ensemble of input neuron combinations available to the arbor of given dimensions, the more appropriate the input neuron combination can be found.

Therefore, we can quantify arbor functionality by the number of different combinations of input neurons available to an arbor of given dimensions. To reduce the arbor functionality to an additive and extensive quantity (i.e., it doubles if L is doubled), we consider the logarithm of the number of accessible input neuron combinations for given arbor dimensions, which we call the *connectivity repertoire*. Thus, maximizing arbor functionality reduces to finding arbor dimensions that maximize the connectivity repertoire.

We computed the connectivity repertoire by adding the following two contributions. First, for given arbor dimensions, we counted all possible different shapes of a dendritic arbor. Each arbor shape selects a different subset of axons that pass within a spine length of a dendrite (Fig. 7.1a). Second, for a given arbor shape, we enumerated the number of combinations of choosing actual axonal inputs out of potential synapses (Fig. 7.1a).

Whereas the second contribution is straightforward to calculate (Stepanyants et al. 2002), the first contribution is challenging because locations of potential synapses are strongly correlated with each other due to the contiguous nature of an arbor. Fortunately, a similar problem has been solved in statistical physics by expressing the astronomical number of different conformations of a branched polymer in terms of its dimensions (Gutin et al. 1993; Rubinstein and Colby 2003). Using this analogy, we derived an expression for the connectivity repertoire, S, in terms of three arbor dimensions (Wen et al. 2009): L, R, and the average distance along the path from the tip of a branch to the cell body, l (Fig. 7.1a),

$$S \sim S_0 + \frac{L}{a}\ln\left(1 - R/l\right) - \frac{l^2}{La} - \frac{L^2}{R^2}. \tag{7.8}$$

Prior to maximizing S in (7.8) with respect to R and l, let us explain the biological meaning of each term. The first term contains contributions independent of R and l (both from variations in arbor shape and from selecting actual synapses out of potential ones) and, thus, will not be considered further.

The second and third terms are R- and l-dependent corrections to the number of different arbor shapes. The second term reflects the fact that straighter branches can come in fewer different shapes (Rubinstein and Colby 2003) and is always negative. As dendrites become straighter, the path length l approaches from above the

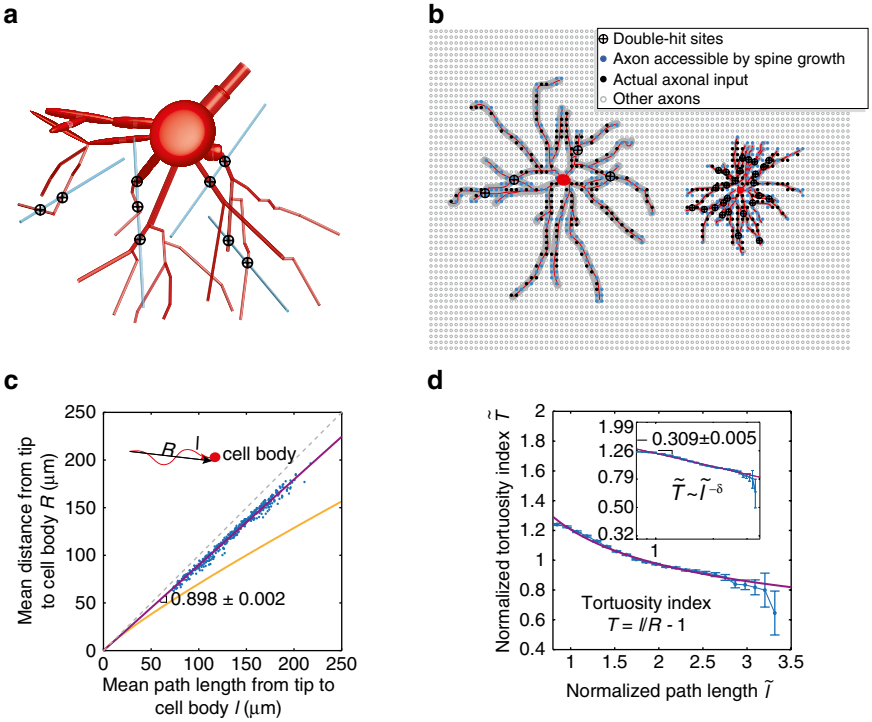

Fig. 7.3 Dendritic arbor shapes reflect maximization of the connectivity repertoire for a given dendritic cost. (**a**) Some axons form multiple potential synapses with a 3D dendritic arbor (*crossed black circles*). (**b**) A sparse arbor, which has lower dendrite density for a given total dendritic length, has fewer multiple potential synapses and, hence, maximizes the connectivity repertoire. (**c**) Tortuosity measured as a function of the average Euclidean distance from the tip of a branch to the cell body on *l*. The best fit (*magenta line*) suggests that basal pyramidal dendrites are approximately straight. Orange line shows tortuous dendrites predicted from maximizing the connectivity repertoire alone, $R \sim a^{1/8} l^{7/8}$. Each point represents a different cell. (**d**) Normalized tortuosity index as a function of the normalized path length from a dendritic segment to cell body. The tortuosity index *T* is defined as the ratio of the length along a path to the Euclidean distance between its ends minus one. In rescaled coordinates, the tortuosity was measured in units of the average index value over all paths within an arbor. The path length was measured in units of the average length over all paths within an arbor as well. *Magenta line* is a power law fit. *Inset* shows the same data on log–log scale. Error bars show s.e.m. This figure is reproduced from Wen et al. (2009)

Euclidian distance between the tip of a branch and the cell body (approximated by *R*), and the second term decreases dramatically. Therefore, maximizing the number of arbor shapes favors $R \ll l$, that is, tortuous branches. The third term reflects the fact that maximizing the number of arbor shapes favors branchy dendrites ($l \ll L$) (Gutin et al. 1993). In these terms, *a* is the persistence length, below which a dendrite cannot bend (Rubinstein and Colby 2003).

The last term in equation is an *R*-dependent correction to the contribution to *S* arising from choosing actual synapses out of potential ones. Some axons could establish more than one potential synapse in different locations on a dendritic arbor (Fig. 7.3a).

If the entire dendritic arbor acts as a unit, differences in the locations of actual synapses from the same axon do not affect the function (Magee and Cook 2000; Chklovskii et al. 2004; Cash and Yuste 1999; Nevian et al. 2007). As a result, additional potential synapses from the same axon are redundant and do not make a contribution to S. Thus, in calculating S, we should subtract the over-counting due to multiple potential synapses, which, for isotropically distributed straight axons (Braitenberg and Schuz 1998; Binzegger et al. 2005; Kisvarday and Eysel 1992), is given by the last term.

Maximizing S favors fewer multiple potential synapses from the same axon and hence smaller last term. Reducing the last term calls for a larger R for a given L or lower dendrite density (Fig. 7.3b). Thus, avoidance of multiple potential synapses leads to a statistical preference for arbors with sparsely distributed branches (Fig. 7.3b).

However, maximization of S alone resulted in more tortuous dendrites than those observed in a pyramidal cell (Fig. 7.3c, yellow line). This fact indicates that the straightness of dendrites (Kawaguchi et al. 2006; Samsonovich and Ascoli 2003; Stepanyants et al. 2004) is driven by reducing the dendritic cost. By taking into account the cost contributed by path length and total wiring length as discussed in the previous section, we derived a scaling form of the cost function $E \sim Ll^{\delta}$, where δ is model dependent (see Appendix).

7.8 Predictions from Functionality–Cost Optimization and Experimental Measurements

Maximizing the connectivity repertoire for a given dendritic cost reduces to maximizing their combination: $S - \beta E$, where β is the weight of E relative to S. We solved this optimization problem (analogous to maximizing entropy for a given energy in statistical physics) and derived analytical expressions relating arbor dimensions l, R, and L. Next, we compare these expressions with experimental measurements.

First, optimal l and R satisfy the relation $l/R - 1 \sim 1/l^{\delta}$, where $l/R - 1$ is defined as the tortuosity index. This prediction is consistent with measurements from basal dendrites of pyramidal cells. The tortuosity index of a path from a dendritic segment to cell body decreases with the path length, and their relationship can be well fit by a power law with exponent $\delta = 0.309 \pm 0.005$ (Fig. 7.3d).

Second, our optimization framework predicts that R and L should satisfy a power law relation $R \sim L^{\nu}$ with the exponent $\nu = 1/(2+\delta)$. Substituting the empirically measured value for δ, we find $\nu = 0.43$. Experimentally, by measuring the arbor dimensions of 2,171 basal pyramidal dendritic arbors, we found that the relation between R and L can be fit via a power law with an exponent, $\nu = 0.44 \pm 0.01$ (Fig. 7.4a), which is not significantly different from our theoretical prediction.

Third, we explored statistical properties of branching by analyzing the spatial correlations among branches within an arbor. To this end, we counted the number of

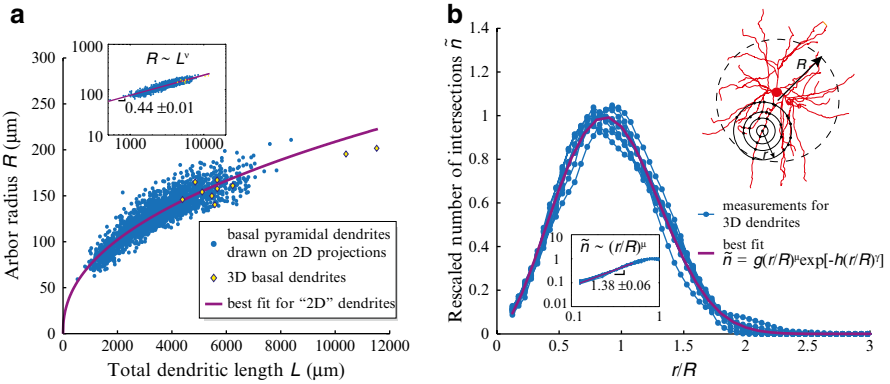

Fig. 7.4 Scaling, universality, and self-similarity of basal dendritic arbors of pyramidal neurons. (**a**) Dendritic arbor radius scales as a power of the total dendritic length. For 2,161 shrinkage-corrected 2D reconstructions of basal dendrites of pyramidal cells from different cortical areas, the power is 0.44 ± 0.01. The ten available shrinkage-corrected 3D reconstructions (Kisvarday and Eysel 1992) are consistent with this relationship. Inset shows the same data on log–log scale. (**b**) Spatial pairwise correlation between dendritic segments for each neuron shown in rescaled coordinates. *Inset* at the *upper right* illustrates how the measurement was performed: counts of intersections between concentric spheres and dendritic branches were averaged over random sphere center locations in the central part of the dendritic arbor. *Curves* corresponding to different neurons collapse onto a master curve, fit by a universal function (*magenta line*), in which μ and γ are the only fitting parameters; coefficients *g* and *h* are fully determined by the normalization conditions. *Inset* under the *main curves* shows the rising part of the plot on log–log scale, indicating a power law relationship and self-similarity of arbor shape. This figure is reproduced from Wen et al. (2009)

pairs of dendritic segments separated by distance r. We expressed the distance in units of R and rescaled the counts, $\tilde{n}$, so that the area under the $\tilde{n}(r/R)$ curve is normalized to one (Fig. 7.4b). The dependence of $\tilde{n}$ on r/R for different arbors collapses onto a single curve (Fig. 7.4b).

The universality of the pairwise correlations in the locations of dendritic segments suggests that dendritic arbors of pyramidal cells are built by statistically similar processes. Indeed, the analogy between our optimization framework and the statistical physics of polymers (Rubinstein and Colby 2003) suggests a functional form of $\tilde{n}$. In particular, the rising part of $\tilde{n}$ would follow a power law $\tilde{n} \sim (r/R)^{\mu}$ (Fig. 7.4b, inset), indicating that a fragment of an arbor is statistically similar to the scaled-down version of the whole arbor (excluding the periphery) (Stevens 2008; Smith et al. 1989; Jelinek et al. 2005; Caserta et al. 1990; Rothnie et al. 2006; Jelinek and Fernandez 1998; Milosevic et al. 2005). These conclusions are further supported by the fact that the measured exponent ν, characterizing the scaling of arbor dimensions across different cells (Fig. 7.4a), and the self-similarity exponent μ (1.38 ± 0.06 and Fig. 7.4b) are consistent with $\mu = 1/\nu - 1$, a relation that results from statistical similarity through a standard scaling argument (see Appendix).

7.9 Why Pyramidal Dendritic Arbors Are Sparser than Purkinje Dendritic Arbors?

We have showed that, in the case of isotropically distributed axons, avoiding multiple potential synapses leads to an arbor territory greater than the total area of the spine-reach zone (Fig. 7.1a). This accounts for the sparseness of basal dendritic arbors of pyramidal cells, which form potential synapses with only a small fraction of axons passing through the arbor territory (Fig. 7.1d, e).

In the case of anisotropic distribution of axons and dendrites, avoidance of multiple potential synapses may not lead to a sparse arbor. For example, if all axons were oriented orthogonally to a planar dendritic arbor, such as parallel fibers and Purkinje cell dendrites in the cerebellum (Llinás et al. 2004), multiple potential synapses could be avoided by arranging dendritic branches so that their spine-reach zones do not overlap. Thus, to minimize the cost of dendrites, the arbor must contract until the spine-reach zone covers most of the arbor territory, just as in Purkinje cell dendrites (Fig. 7.1c). Although a projection of Purkinje dendritic arbor on the direction other than that of parallel fibers would contain many overlaps of the spine-reach zone, this would not generate multiple potential synapses for parallel fibers.

7.10 Discussion

Are our results applicable to cell classes other than pyramidal and Purkinje cells? We note that the basic aspects of our theory still hold even if some assumptions were relaxed. (a) If presynaptic axons are tortuous and/or branchy rather than straight on the scale of a dendritic arbor, our theory would still hold but predict different scaling exponents. (b) If an individual dendritic branch rather than the whole arbor acts as a unit (Losonczy and Magee 2006; Poirazi et al. 2003a, b), actual synapses from the same axon lead to the same functionality only when they occur on the same branch. In this case, calculations would be different but the general framework would still hold.

However, arbor shapes would fall outside the current theoretical framework in the following cases. (a) Instead of maximizing the connectivity repertoire, the objective of some dendrites could be to maximize the number of synaptic contacts with the same presynaptic neuron. An example includes large monopolar cells in the insect optic lobe innervated by photoreceptors (Nicol and Meinertzhagen 1982). (b) Spatial distribution of axons from appropriate input neurons may not be a priori unknown to the arbor but partially or fully predetermined. For example, layer V apical dendrites reach out to upper cortical layers I–III containing appropriate inputs, which is why we restricted our analysis to basal dendritic arbors. To determine whether our theory is applicable to various cell types, large data sets of high-quality arbor reconstructions would be desirable.

Why do we believe that the distribution of axons presynaptic to basal pyramidal dendrites is not predetermined? (a) Specificity in the location of pyramidal axons has been demonstrated only on the scale of cortical layers and columns, which is greater than the radius of a basal dendritic arbor (~100 μm) (Gilbert and Wiesel 1989; Mooser et al. 2004). (b) On the smaller scale (<100 μm), pyramidal axons follow relatively straight trajectories in various directions (Binzegger et al. 2005; Stepanyants et al. 2004; Fujita and Fujita 1996; Lund et al. 1993; Anderson et al. 2002; Kisvarday and Eysel 1992) and, thus, are unlikely to organize into specific patterns. (c) As synapses on a pyramidal dendrite are made about every half micron, it is unclear how axons from appropriate input neurons could align along dendrites in such a precise manner. Even if this arrangement could be achieved for one dendritic arbor, thousands of other arbors present in the dendritic territory would require a rearrangement of axons from one dendrite to the next, a scenario that is highly improbable.

One may question the validity of our assumption that pyramidal cell dendrites avoid multiple potential synapses because experiments indicate that synaptically coupled cortical neurons share multiple synaptic contacts (Markram et al. 1997; Silver et al. 2003). However, this observation does not contradict our theory for two reasons. First, electrophysiological recordings are heavily biased towards connected and hence nearby neurons. Although nearby neurons may make many potential synapses, these inputs are in a minority. Indeed, in V1, 83 % of synapses on a dendrite originate from neurons located farther than 200 μm in the cortical plane (Stepanyants et al. 2009). For these presynaptic neurons, typically only one axonal branch courses through the dendritic arbor territory and hence is unlikely to make multiple potential synapses. Second, it is possible that various synaptic contacts form independently according to some local rules. Therefore, development can only strive to avoid multiple potential synapses but cannot guarantee their complete absence.

The cornerstone of our theory is the idea that a dendritic arbor avoids multiple hits with the same axon. Statistically, such avoidance results in an apparent repulsion between branches. To go beyond our teleological theory and speculate developmental mechanisms responsible for repulsion, we must distinguish the following two logical possibilities. First, growing dendrites may experience some kind of interaction, which forces them to become more extended, thus leading to reduction of multiple hits. Second, arbors somehow detect multiple hits with the same axon and rearrange their shapes in response. We think that the latter possibility is less realistic, not only because it would be difficult for a cell to detect multiple hits from the same axon on the background of simultaneous signals from thousands of other inputs, but also mostly because dendrites should avoid multiplying even potential synapses which generate no electrical signal in dendrites. We therefore think that the first possibility—avoidance of multiple hits as a consequence of interaction between branches—is more realistic.

Although the mechanism for such interaction among dendrites is unknown in vertebrates, it has been discovered in invertebrates in the form of homophilic Dscam interaction (Samsonovich and Ascoli 2003; Hattori et al. 2007; Schmucker et al.

2000; Hughes et al. 2007). Due to a large number of stochastically chosen splice isoforms, this molecule can mediate self-repulsion among branches of the same neuron without inducing interactions among different neurons. However, Dscams are thought to be nondiffusible and hence incapable of acting over long distances. Moreover, a vertebrate homolog of invertebrate Dscam does not have a large number of splice isoforms (Fuerst et al. 2008; Yamagata and Sanes 2008). We conjecture that a diffusible molecule with a large number of isoforms mediates self-repulsion in vertebrates.

Prior works on understanding arbor shape have involved computer simulations (Samsonovich and Ascoli 2003, 2005; van Pelt and Uylings 2002) using specific rules of branching and orientation of dendrites. Interestingly, it was suggested that reproducing realistic arbor shape requires effective repulsion between the cell body and dendrites (Samsonovich and Ascoli 2003). Although the proposed scheme can explain the straightness of dendritic branches and their centripetal orientation (Samsonovich and Ascoli 2003; Marks and Burke 2007a), it does not account for the distribution of the nearest neighbor distance among branches (Marks and Burke 2007b). Here, based on the analysis of dendritic functionality, we proposed that effective repulsion exists among all segments of a dendritic arbor, not just between the cell body and dendrites.

More recently, Hermann Cuntz and colleagues (Cuntz 2012; Cuntz et al. 2010, 2012) have used a greedy optimization algorithm to generate realistic dendritic arbor shapes with a variability that matches different neuronal types in the insect and mammalian brains (see Chap. 6). In his approach, an in silico arbor must calculate a strategy to minimize both the total wire length and path length cost while connecting given target points in the neuropil with defined spatial distribution. Our complementary approaches reach similar conclusions that total wire length and path length costs are important for determining the shape of an arbor. In the future, however, it is important to understand how these target points (or seeds) are chosen. Do these target points reflect the location of the most appropriate axonal inputs? If so, what determines their sparseness and spatial distribution? These questions would be answered if we have a better understanding of the organization and connectivity of a neuropil on the size of a dendritic arbor.

Finally, the idea that avoidance of multiple hits affects arbor shape may not be limited to neurons and apply to other biological objects. Consider, for example, the spatial arrangement of tree branches. As a tree strives to maximize its exposure to sunlight, its leaves must avoid shading each other (Mauseth 2003; Thomas 2001). This means that the branches should minimize multiple hits with straight lines directed from the sun. Because light rays come from varying directions, they induce repulsion among branches, similarly to self-repulsion in dendritic arbors of pyramidal cells. As the cost of branches is likely to grow with both the total length and the path length, our theory should apply to the spatial distribution of tree branches as well. Thus the similarity of shapes among neurons and trees may not be a coincident but arises from similar evolutionary objectives.

Appendix

A.1 Relation Between Scaling Exponents

If the statistical properties of different dendritic arbors were universal and dendritic arbors were indeed self-similar, the scaling exponent, ν, from the power law between R and L, would be related to the exponent from the rising part of spatial pairwise correlation function between dendritic segments, μ, as shown below.

For self-similar dendritic arbors built by common rules, the rising part of the pairwise correlation function on the regular scale, $n(r)$, would be described by the power law function

$$n \sim r^{\mu}, r < R. \tag{7.9}$$

In addition, the pairwise correlation function would be characterized by a single length scale, R. Specifically, if $n(r)$ decays fast for $r>R$ and the rising part of $n(r)$ remains a power law until r is on the order of R (as in agreement with our data), then the normalization condition $\int_0^{\infty} n(r)\,dr = L$ can be well approximated by introducing a cutoff R:

$$\int_0^{R} n(r)\,dr \approx L. \tag{7.10}$$

By using (7.9) for $n(r)$ in (7.10), we obtain

$$L \sim R^{\mu+1}. \tag{7.11}$$

Recall that our measurement for arbor dimensions shows $R \sim L^{\nu}$ (Fig. 7.4a). Therefore, we arrive at a relation between exponents μ and ν:

$$\mu = \frac{1}{\nu} - 1. \tag{7.12}$$

In addition, given (7.9) and (7.12), the rising part of the rescaled pairwise correlation function should follow a similar power law $\tilde{n} \sim (r/R)^{\mu}$. This can be derived straightforwardly from the relation $\tilde{n} = nR/L$, which is a consequence of the normalization conditions.

A.2 A Cost Model for Dendritic Arbors

As maximizing the connectivity repertoire alone leads to more tortuous branches than observed, we must include the dendritic cost in the optimization framework.

After considering several simplified models based on the above reasoning (Wen and Chklovskii 2008), we propose that the cost scales with L and l as

$$E \sim Ll^{\delta}. \tag{7.13}$$

The value of exponent δ is model dependent. Below, we consider one simplified model that yields a specific value of δ.

We assume that E is proportional to the total area of dendritic surface for the following reason. To maintain the resting potential of a neuron or low [Na+] inside a cell, sodium ions permeating into a neuron should be actively extruded by Na+/K+ pumps (Attwell and Laughlin 2001). The amount of ATP expended is proportional to the membrane capacitance for action potential propagation or membrane input conductance in the absence of spikes (Attwell and Laughlin 2001). Hence, in both considerations, E is proportional to the membrane surface area,

$$E \sim Ld, \tag{7.14}$$

where d is the mean dendritic diameter.

Although E decreases as the mean dendritic diameter d is reduced, a small diameter would detrimentally affect dendritic function. One possible reason is that proteins must be transported from the cell body to synapses and the rate of transport is proportional to the number of microtubules at a given cross section of a dendrite (Hillman 1979). The rate of protein transport through a cross section must be proportional to the number of synapses downstream of that cross section. If the density of microtubules (per cross-sectional area) is roughly invariant, the cross-sectional area must be proportional to the number of microtubules and hence to the number of synapses downstream (Hsu et al. 1998; Hillman 1979; Wittenberg and Wang 2007). If the typical branch has length l, the number of synapses on it is Nl/L. Therefore, a typical dendritic diameter is

$$d^2 \sim ANl / L, \tag{7.15}$$

where A is a cross-sectional area needed to support one synapse. By substituting (7.15) with (7.14), we find that

$$E \sim N^{1/2} L^{1/2} l^{1/2}. \tag{7.16}$$

Given that $N \sim L$ (Larkman 1991), we obtain

$$E \sim Ll^{1/2}. \tag{7.17}$$

References

Anderson JC, Binzegger T, Douglas RJ, Martin KA (2002) Chance or design? Some specific considerations concerning synaptic boutons in cat visual cortex. J Neurocytol 31(3–5): 211–229

Ascoli GA (2006) Mobilizing the base of neuroscience data: the case of neuronal morphologies. Nat Rev Neurosci 7(4):318–324

Attwell D, Laughlin SB (2001) An energy budget for signaling in the grey matter of the brain. J Cereb Blood Flow Metab 21(10):1133–1145

Binzegger T, Douglas RJ, Martin KA (2005) Axons in cat visual cortex are topologically self-similar. Cereb Cortex 15(2):152–165

Braitenberg V, Schuz A (1998) Cortex: statistics and geometry of neuronal connectivity. 2nd thoroughly rev. edn. Springer, New York

Caserta F, Stanley HE, Eldred WD, Daccord G, Hausman RE, Nittmann J (1990) Physical mechanisms underlying neurite outgrowth: a quantitative analysis of neuronal shape. Phys Rev Lett 64(1):95–98

Cash S, Yuste R (1999) Linear summation of excitatory inputs by CA1 pyramidal neurons. Neuron 22(2):383–394

Chklovskii DB, Mel BW, Svoboda K (2004) Cortical rewiring and information storage. Nature 431(7010):782–788

Chklovskii DB, Vitaladevuni S, Scheffer LK (2010) Semi-automated reconstruction of neural circuits using electron microscopy. Curr Opin Neurobiol 20(5):667–675

Cuntz H (2012) The dendritic density field of a cortical pyramidal cell. Front Neuroanat 6:2

Cuntz H, Borst A, Segev I (2007) Optimization principles of dendritic structure. Theor Biol Med Model 4:21

Cuntz H, Forstner F, Borst A, Häusser M (2010) One rule to grow them all: a general theory of neuronal branching and its practical application. PLoS Comput Biol 6(8)

Cuntz H, Mathy A, Häusser M (2012) A scaling law derived from optimal dendritic wiring. Proc Natl Acad Sci USA 109(27):11014–11018

Denk W, Horstmann H (2004) Serial block-face scanning electron microscopy to reconstruct three-dimensional tissue nanostructure. PLoS Biol 2(11):e329

Fuerst PG, Koizumi A, Masland RH, Burgess RW (2008) Neurite arborization and mosaic spacing in the mouse retina require DSCAM. Nature 451(7177):470–474

Fujita I, Fujita T (1996) Intrinsic connections in the macaque inferior temporal cortex. J Comp Neurol 368:467–486

Gilbert CD, Wiesel TN (1989) Columnar specificity of intrinsic horizontal and corticocortical connections in cat visual cortex. J Neurosci 9(7):2432–2442

Gutin AM, Grosberg AY, Shakhnovich EI (1993) Polymers with annealed and quenched branchings belong to different universality classes. Macromolecules 26(6):1293–1295

Hattori D, Demir E, Kim HW, Viragh E, Zipursky SL, Dickson BJ (2007) Dscam diversity is essential for neuronal wiring and self-recognition. Nature 449(7159):223–227

Hillman D (1979) Neuronal shape parameters and substructures as a basis of neuronal form. In: The Neurosciences: fourth study program. MIT Press, Cambridge, MA, pp vii, 1185 p

Hsu A, Tsukamoto Y, Smith RG, Sterling P (1998) Functional architecture of primate cone and rod axons. Vision Res 38(17):2539–2549

Hughes ME, Bortnick R, Tsubouchi A, Baumer P, Kondo M, Uemura T, Schmucker D (2007) Homophilic Dscam interactions control complex dendrite morphogenesis. Neuron 54(3):417–427

Jelinek H, Elston GN, Zietsch B (2005) Fractal analysis: pitfalls and revelations in neuroscience. In: Losa GA, Merlini D, Nonnenmacher TF, Weibel ER (eds) Fractals in biology and medicine, vol 4. Birkhauser Verlag AG, Switzerland, pp 85–94

Jelinek HF, Fernandez E (1998) Neurons and fractals: how reliable and useful are calculations of fractal dimensions? J Neurosci Methods 81(1–2):9–18

Kawaguchi Y, Karube F, Kubota Y (2006) Dendritic branch typing and spine expression patterns in cortical nonpyramidal cells. Cereb Cortex 16(5):696–711

Kisvarday ZF, Eysel UT (1992) Cellular organization of reciprocal patchy networks in layer III of cat visual cortex (area 17). Neuroscience 46(2):275–286

Kleinfeld D, Bharioke A, Blinder P, Bock DD, Briggman KL, Chklovskii DB, Denk W, Helmstaedter M, Kaufhold JP, Lee WC, Meyer HS, Micheva KD, Oberlaender M, Prohaska S, Reid RC, Smith SJ, Takemura S, Tsai PS, Sakmann B (2011) Large-scale automated histology in the pursuit of connectomes. J Neurosci 31(45):16125–16138

Larkman AU (1991) Dendritic morphology of pyramidal neurones of the visual cortex of the rat: III. Spine distributions. J Comp Neurol 306(2):332–343

Lichtman JW, Livet J, Sanes JR (2008) A technicolour approach to the connectome. Nat Rev Neurosci 9(6):417–422

Llinás RR, Walton KD, Lang EJ (2004) Cerebellum. In: Shepherd GM (ed) The synaptic organization of the brain, 5th edn. Oxford University Press, New York, p xiv, 719 p

Losonczy A, Magee JC (2006) Integrative properties of radial oblique dendrites in hippocampal CA1 pyramidal neurons. Neuron 50(2):291–307

Lund JS, Yoshioka T, Levitt JB (1993) Comparison of intrinsic connectivity in different areas of macaque monkey cerebral cortex. Cereb Cortex 3:148–162

Magee JC, Cook EP (2000) Somatic EPSP amplitude is independent of synapse location in hippocampal pyramidal neurons. Nat Neurosci 3(9):895–903

Markram H, Lubke J, Frotscher M, Roth A, Sakmann B (1997) Physiology and anatomy of synaptic connections between thick tufted pyramidal neurones in the developing rat neocortex. J Physiol 500(Pt 2):409–440

Marks WB, Burke RE (2007a) Simulation of motoneuron morphology in three dimensions. I. Building individual dendritic trees. J Comp Neurol 503(5):685–700

Marks WB, Burke RE (2007b) Simulation of motoneuron morphology in three dimensions. II. Building complete neurons. J Comp Neurol 503(5):701–716

Martone ME, Zhang S, Gupta A, Qian X, He H, Price DL, Wong M, Santini S, Ellisman MH (2003) The cell-centered database: a database for multiscale structural and protein localization data from light and electron microscopy. Neuroinformatics 1(4):379–395

Mauseth JD (2003) Botany : an introduction to plant biology, 3rd edn. Jones and Bartlett Publishers, Boston

Milosevic NT, Ristanovic D, Stankovic JB (2005) Fractal analysis of the laminar organization of spinal cord neurons. J Neurosci Methods 146(2):198–204

Mooser F, Bosking WH, Fitzpatrick D (2004) A morphological basis for orientation tuning in primary visual cortex. Nat Neurosci 7(8):872–879

Napper RM, Harvey RJ (1988a) Number of parallel fiber synapses on an individual Purkinje cell in the cerebellum of the rat. J Comp Neurol 274(2):168–177

Napper RM, Harvey RJ (1988b) Quantitative study of the Purkinje cell dendritic spines in the rat cerebellum. J Comp Neurol 274(2):158–167

Nevian T, Larkum ME, Polsky A, Schiller J (2007) Properties of basal dendrites of layer 5 pyramidal neurons: a direct patch-clamp recording study. Nat Neurosci 10(2):206–214

Nicol D, Meinertzhagen IA (1982) An analysis of the number and composition of the synaptic populations formed by photoreceptors of the fly. J Comp Neurol 207(1):29–44

Poirazi P, Brannon T, Mel BW (2003a) Arithmetic of subthreshold synaptic summation in a model CA1 pyramidal cell. Neuron 37(6):977–987

Poirazi P, Brannon T, Mel BW (2003b) Pyramidal neuron as two-layer neural network. Neuron 37(6):989–999

Ramón y Cajal S (1899) Textura del Sistema Nervioso del Hombre y de los Vertebrados (Texture of the nervous system of man and the vertebrates), vol 1. Springer, New York

Rapp M, Segev I, Yarom Y (1994) Physiology, morphology and detailed passive models of guinea-pig cerebellar Purkinje cells. J Physiol 474(1):101–118

Rothnie P, Kabaso D, Hof PR, Henry BI, Wearne SL (2006) Functionally relevant measures of spatial complexity in neuronal dendritic arbors. J Theor Biol 238(3):505–526

Rubinstein M, Colby RH (2003) Polymer physics. Oxford University Press, Oxford, NY
Samsonovich AV, Ascoli GA (2003) Statistical morphological analysis of hippocampal principal neurons indicates cell-specific repulsion of dendrites from their own cell. J Neurosci Res 71(2):173–187
Samsonovich AV, Ascoli GA (2005) Statistical determinants of dendritic morphology in hippocampal pyramidal neurons: a hidden Markov model. Hippocampus 15(2):166–183
Schmucker D, Clemens JC, Shu H, Worby CA, Xiao J, Muda M, Dixon JE, Zipursky SL (2000) Drosophila Dscam is an axon guidance receptor exhibiting extraordinary molecular diversity. Cell 101(6):671–684
Shepherd GM, Svoboda K (2005) Laminar and columnar organization of ascending excitatory projections to layer 2/3 pyramidal neurons in rat barrel cortex. J Neurosci 25(24):5670–5679
Silver RA, Lubke J, Sakmann B, Feldmeyer D (2003) High-probability uniquantal transmission at excitatory synapses in barrel cortex. Science 302(5652):1981–1984
Sjöström PJ, Turrigiano GG, Nelson SB (2001) Rate, timing, and cooperativity jointly determine cortical synaptic plasticity. Neuron 32(6):1149–1164
Smith TG Jr, Marks WB, Lange GD, Sheriff WH Jr, Neale EA (1989) A fractal analysis of cell images. J Neurosci Methods 27(2):173–180
Stepanyants A, Hof PR, Chklovskii DB (2002) Geometry and structural plasticity of synaptic connectivity. Neuron 34(2):275–288
Stepanyants A, Martinez LM, Ferecsko AS, Kisvarday ZF (2009) The fractions of short- and long-range connections in the visual cortex. Proc Natl Acad Sci USA 106(9):3555–3560
Stepanyants A, Tamas G, Chklovskii DB (2004) Class-specific features of neuronal wiring. Neuron 43(2):251–259
Stevens CF (2008) All arbors have the same shape. In: Neuronal circuits: from structure to function, CSHL and private communication, 2008
Thomas PA (2001) Trees: their natural history, 1st edn. Cambridge University Press, UK
Thomson AM, Bannister AP (2003) Interlaminar connections in the neocortex. Cereb Cortex 13(1):5–14
Trachtenberg JT, Chen BE, Knott GW, Feng G, Sanes JR, Welker E, Svoboda K (2002) Long-term in vivo imaging of experience-dependent synaptic plasticity in adult cortex. Nature 420(6917):788–794
van Pelt J, Uylings HB (2002) Branching rates and growth functions in the outgrowth of dendritic branching patterns. Network 13(3):261–281
Vetter P, Roth A, Häusser M (2001) Propagation of action potentials in dendrites depends on dendritic morphology. J Neurophysiol 85(2):926–937
Wen Q, Chklovskii DB (2008) A cost-benefit analysis of neuronal morphology. J Neurophysiol 99(5):2320–2328
Wen Q, Stepanyants A, Elston GN, Grosberg AY, Chklovskii DB (2009) Maximization of the connectivity repertoire as a statistical principle governing the shapes of dendritic arbors. Proc Natl Acad Sci USA 106(30):12536–12541
Wittenberg GM, Wang SS-H (2007) Evolution and scaling of dendrites. In: Stuart G, Spruston N, Häusser M (eds) Dendrites, 2nd edn. Oxford University Press, USA, pp 43–67
Yamagata M, Sanes JR (2008) Dscam and Sidekick proteins direct lamina-specific synaptic connections in vertebrate retina. Nature 451(7177):465–469